Microstructure, Tensile Properties and Fracture Behavior of HPDC Magnesium Alloy AZ91

Zixi Sun, Xinyu Geng, Luyang Ren, and Henry Hu

***Abstract*—Understanding of tensile and fracture behaviours of die cast magnesium alloys is of importance for proper design of various emerging automotive applications. In the present study, magnesium alloy AZ91 was high pressure die cast into rectangular coupons with section thicknesses of 2, 6 and 10 mm. The effect of section thicknesses on strain-hardening and fracture behaviours of the die cast AZ91 was investigated. The results of tensile testing indicate that the ultimate tensile strength (UTS), yield strength (YS), elongation (e_f), modulus, toughnrss and resilience decrease to 129.17, 110.59 MPa, 0.37%, 25.9 GPa, 0.89 MJ/m^3, and 236.10 kJ/m^3 from 245.54, 169.26 MPa, 4.07%, 37.8 GPa, 8.34 MJ/m^3, and 378.95 kJ/m^3 with increasing section thicknesses of die cast AZ91 to 10 mm from 2 mm, respectively. The analysis of true stress vs. strain curves shows that the straining hardening rates during the plastic deformation of the alloy increase to 5500 MPa from 4600 MPa with decreasing the section thickness to 2 mm from 10 mm, respectively. The microstructure analyses by the optical microscopy (OM) and scanning electron microscopy (SEM) reveal that the high tensile properties should be attributed the low porosity level, fine dendrite structure, high eutectic content, and thick skin. The observation via SEM fractography illustrates that the fracture behaviour of die cast AZ91 is influenced by section thicknesses. As the section thickness increases, the fracture of AZ91 tends to transit from ductile to brittle mode due to arising porosity content and coarsening microstructure.**

***Index Terms*—Magnesium alloy AZ91, high pressure die casting, tensile and fracture behaviors, microstructure.**

I. Introduction

Magnesium usage in automobiles has arisen significantly due to consumer demands for increased performance and fuel economy of vehicles. Most magnesium applications presently used in the automotive industry are high-pressure die cast (HPDC), and have relatively good strengths and high ductility at room temperature. Applications of HPDC magnesium alloys, such as front end support assemblies, steering wheel armatures and steering column support brackets [1], [2], have not only complex shapes but also cross sections with various thicknesses. Very often, under normal die casting conditions, thick sections have a higher tendency to solidification shrinkage and porosity caused by inclusion of gas than thin walls. It has been indicated [3]-[6] that the porosity level of HPDC Mg alloys influences mechanical properties, such as ultimate tensile strength (UTS), 0.2% yield strength (YS) and elongation (e_f). Cáceres *et al.* [7] attempted to establish the relationship between the hardness and yield strength for the HPDC AZ91 with the section thickness upto 5 mm, while the study by Sin *et al.* [8] showed the tensile properties of the plaster mold cast AZ91 with the section thicknesses of 1 to 4.3 mm, which were compared with those of the HPDC counterpart. Gjestland *et al.* [9] present the tensile properties of the HPDC AZ91 alloy with the section thicknesses varying from 1 to 9 mm, but failed to provide detailed analyses of plastic deformation, and tensile and fracture behaviors.

This paper presents an in-depth analysis of strain-hardening behaviour during plastic deformation and fracture characteristics of the HPDC AZ91 alloy with section thicknesses of 2, 6 and 10 mm. The influence of section thicknesses on plastic deformation behaviour of the alloy was studied based on the analysis of true stress-strain relation. The fracture behaviour of the HPDC AZ91 affected by section thicknesses was characterized by using SEM fractography.

II. Experimental Procedures

A. Alloy and Casting Preparation

The magnesium alloy selected in this study was die casting Mg-8.48 wt.%Al-0.61 wt.%Zn-0.18 wt.%Mn alloy AZ91D. Flat rectangular coupons of 125 mm × 27 mm with different section thicknesses of 2, 6 and 10 mm were die cast on a 700 ton cold chamber horizontal high pressure die casting machine.

B. Porosity Measurement

Porosity contents of specimens was measured based on Archimedes principle. After specimen weights were measured in air and distilled water, Equation (1) was used to calculated the actual density (ρ_a) of each specimen according to ASTM Standard D3800:

$$\rho_a = \frac{W_a \times \rho_w}{W_a - W_w} \tag{1}$$

where W_a equals to weight in air and W_w equals to weights in water, and ρ_w equals to density of water. Equation (2) was applied for computing the porosity percentage (P%) according to ASTM Standard C948:

$$P\% = \frac{\rho_t - \rho_a}{\rho_t} \times 100\% \tag{2}$$

where ρ_t is the theoretical density of the alloy AZ91, i.e.,

Manuscript received May 20, 2019; revised January 13, 2020.

The authors are with Department of Mechanical, Automotive & Material Engineering, University of Windsor, Windsor, ON N9B 3P4 Canada (e-mail: sun13h@uwindsor.ca, gengx@uwindsor.ca, ren11h@uwindsor.ca, huh@uwindsor.ca).

doi: 10.18178/ijmmm.2020.8.2.483

1810 kg/cm^3 [5].

C. Tensile Testing

The mechanical properties of the HPDC AZ91 alloy with various thickness were evaluated by tensile tests, which were performed at ambient temperature on an Instron machine equipped with a computer data acquisition system. Following ASTM B557, subsize flat tensile specimens (25 mm in gage length, 6 mm in width, and 2, 6, 10 mm in as-cast thicknesses) were machined from the die cast coupons. The tensile properties, including 0.2% yield strength (YS), ultimate tensile strength (UTS), and elongation at fracture (e_f), were obtained based on the average of three tests.

D. Characterization of Microstructure and Fractured Surface

Specimens were sectioned, mounted, and polished from the center of the coupons and prepared following the standard metallographic procedures. An etchant of 60% ethanal-20% acetic acid-19% distilled water-1% nitric acid was applied to polished specimens for microscopic examination. A Buehler optical image analyzer 2002 system was used to determine primary characteristics of the specimens. The detailed features of the microstructure were also characterized at high magnifications by a scanning electron microscope (SEM), Hitachi Tabletop Microscope TM3000, with a maximum resolution of 30 nm in a backscattered mode (BSE)/1 μm in x-ray diffraction mapping mode, and useful magnification of 10–30,000.

III. Results and Discussion

A. Porosity Content

Fig. 1 presents the SEM micrographs, showing the porosity contents in the HPDC AZ91 alloy. Despite the presence of very few and small pores in the 2 mm specimens as shown in Fig. 1(a), a large number of big pores are easily observed in both the 6 and 10 mm specimens as illustrated in Fig. 1(b) and Fig. 1(c).

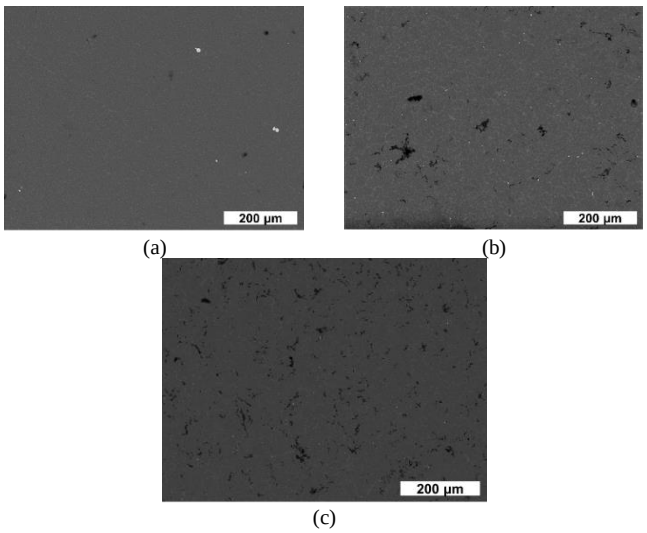

(a) (b) (c)

Fig. 1. SEM micrographs showing porosity in the die cast AZ91 alloy with section thicknesses of (a) 2 mm, (b) 6 mm, and (c) 10 mm.

The porosity contents of the HPDC AZ91 alloy specimens with the section thicknesses of 2 mm, 6 mm and10 mm are presented in Fig. 2. The 6 and 10 mm specimens have the high porosity contents of 2.61 % and 3.57 %, respectively, while there is a very low porosity content of only 0.53% in the 2 mm coupon. Examination of the measured porosity contents reveals the variation in casting quality resulting from differences in section thicknesses. When the casting section becomes thin, the porosity content of the HPDC AZ91 alloy decreases, and the size of the entrapped pores reduces.

The rapid cavity filling of liquid metal into the die and high solidification rates lead to the formation of the small pores and the low content of porosity in the 2 mm coupon. The implication from computer simulation of mold filling and heat transfer of the HPDC AZ91 alloy indicates that the existence of high porosity contents in the thick 6 and 10 mm specimens might be attributed to the improper filling pattern and slow solidification [10].

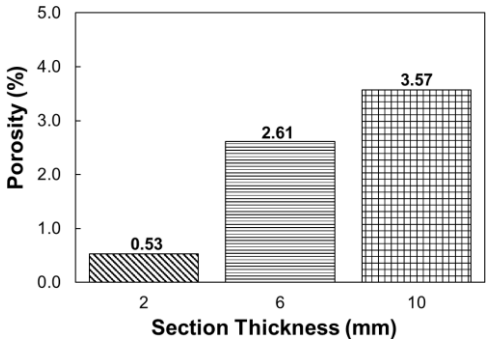

Fig. 2. Porosity content vs. section thicknesses.

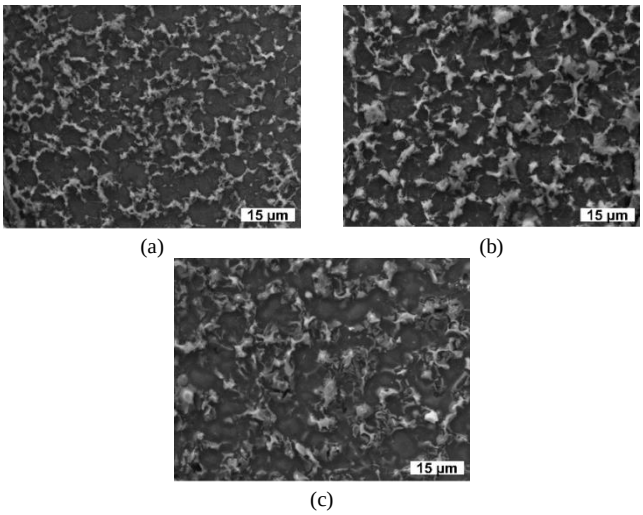

(a) (b) (c)

Fig. 3. SEM micrograph showing microstructure in the outer skin of the die cast AZ91 alloy with difference wall thicknesses, (a) 2, (b) 6 and (c) 10 mm, respectively.

B. Dendrite Measurement

Fig. 3 gives SEM micrographs showing the existence of a fine microstructure in the outer skins of the HPDC AZ91 alloy for the 2, 6 and 10 mm specimens. The dendrite sizes in the outer skins of the HPDC AZ91 alloy are 6, 15 and 20 μm for the 2, 6 and 10 mm specimens, respectively. The dendritic structure in the center of the AZ91 coupons are present in Fig. 4. It can be seen from Fig. 4(a) that the dendrite size in the center of the 2 mm is only 14 μm and still small. However, there are large primary α-Mg dendrites (32 μm) in the center of the 10 mm specimen. Fig. 5 summarizes the average size of primary α-Mg dendrites in different

region of each section thickness. The reduction in the section thickness decreases the dendrite size considerably, although the variation of the dendritic structure is insignificant in the outer skins.

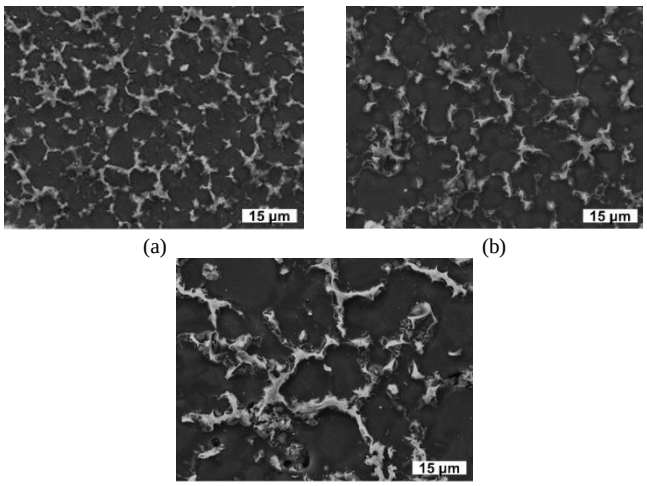

(a) (b)

(c)

Fig. 4. SEM micrograph showing microstructure in the center of the die cast AZ91 alloy with difference wall thicknesses, (a) 2, (b) 6 and (c) 10 mm, respectively.

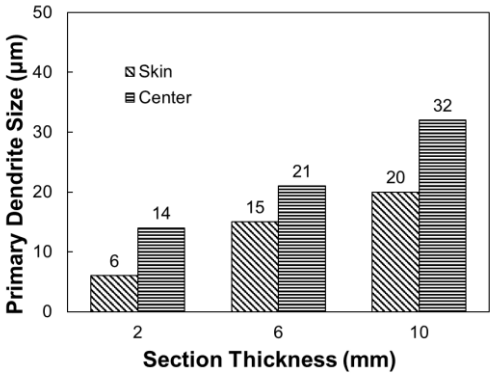

Fig. 5. Average primary dendrite size in the out skin and center of the die cast AZ91 alloy with the section thicknesses of 2, 6 and 10 mm.

The relation between the skin thickness in the skin area, and section thicknesses is shown in Fig. 6. With the section thickness increase, more gas is entrapped into the die and the tendency to form shrinkage porosity is also become high. As the die temperature is constant for all three thicknesses coupons, the cooling rate is almost the same for all three coupons at the very beginning of solidification. As solidification keeps on going, the thicker specimen tends to release more latent heat, which reduces the solidification rate. As a result, more shrinkage porosity and thinner skin tends to forms in the thick specimens.

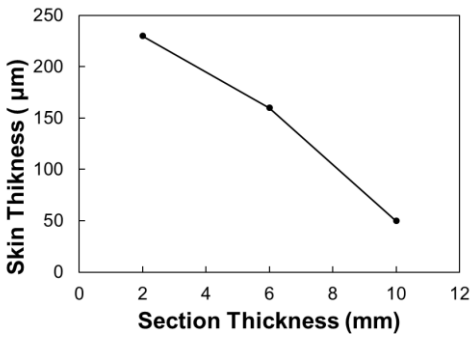

Fig. 6. Skin Thickness vs. Section Thickness.

To understand the development of the observed microstructure of the HPDC AZ91, the filling and solidification sequences of the conventional HPDC process need to be taken into consideration. The process starts with pouring the liquid metal at a desired temperature into a shot sleeve. The direct contact between the liquid metal and the sleeve chills the metal rapidly to its liquidus temperature, and kicks off solidification. The formation of a large volume fraction of the primary α-Mg dendrite occurs in the sleeve prior to the metal arrives at the gate of the die cavity. Once the partially-solidified metal is pushed into the cavity, the pre-formed α-Mg crystals floats in the melt, which stays in the finally-solidified microstructure [5]. Due to the fast cooling at the interface between the casting and die, the surface of the specimens become the location to form fine grains. In the center of the specimens, the solidification for the 6 and 10 mm thick specimen due to their thick section thickness takes place much more slowly than that of the 2 mm specimen. As a result, the coarse microstructure developed in the center of the10 mm thick specimen.

C. Eutectic Content

Fig. 7 presents the SEM images in BSE mode showing the etched microstructure of the AZ91 alloy in details at a high magnification. The results of the EDS analysis as shown in Fig. 8 and the element analysis in atomic percentages listed in Table I indicate that the microstructure of the etched AZ91 consists of primary α-Mg grains (dark), eutectic β-$Mg_{17}Al_{12}$ phases (bright), and Al-Mn intermetallics (white spot). The eutectic β-$Mg_{17}Al_{12}$ phases and Al-Mn intermetallics are present in the form of isolated fine particles surrounding the boundaries of the primary α-Mg grains.

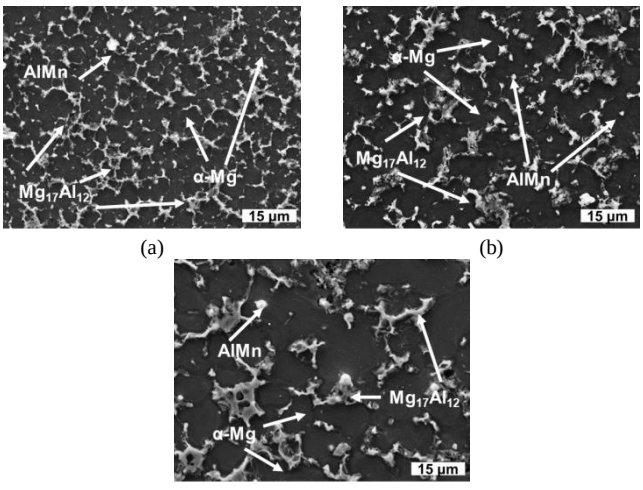

(a) (b)

(c)

Fig. 7. SEM micrographs in BSE mode showing constituent phases in the microstructure of the die cast AZ91 alloy (a) 2, (b) 6 and (c) 10 mm.

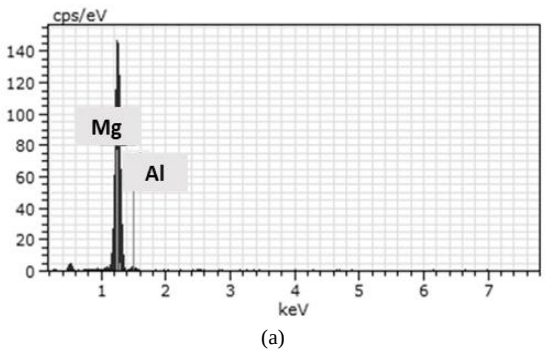

(a)

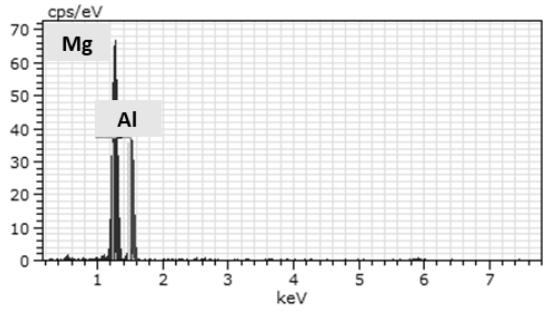

(b)

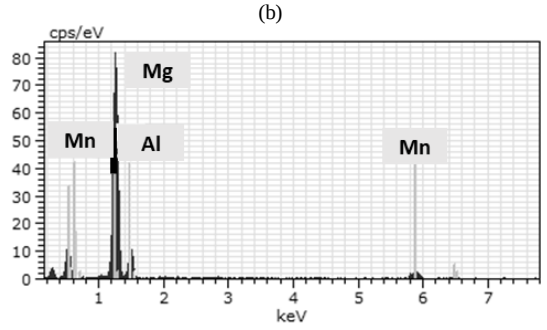

(c)

Fig. 8. EDS spectra (a), (b) and (c) for the areas containing α-Mg grains (dark), and β-$Mg_{17}Al_{12}$ phases (bright), and Al-Mn intermetallic (white spots) as shown in Fig. 7 (a), respectively.

TABLE I: ELEMENTS IN ANALYZED PHASES SHOWN IN FIG. 5

Phase	Element	Atomic (at. %)
α-Mg	Mg	96.68
	Al	3.32
$Mg_{17}Al_{12}$	Mg	57.15
	Al	42.85
AlMn	Mg	56.57
	Al	26.48
	Mn	16.95

Fig. 9 presents the converted micrographs from Fig. 7, highlighting the presence of the $Mg_{17}Al_{12}$ eutectics in the observed alloys represented by the black area. Shown in Fig. 9, the image analysis reveals that the volume fraction of the intermetallic phases decrease with increasing the section thickness. Fig. 10 shows the variation of the volume fraction of the eutectics with the different section thickness. The volume fractions of the intermetallic phases in 2, 6 and 10 mm are measured to be 19.86%, 16.71% and 14.91%, respectively.

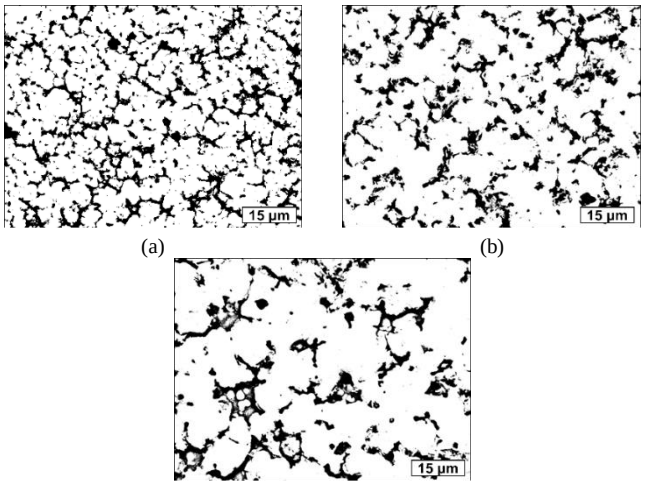

(a) (b)

(c)

Fig. 9. Binary black and white images showing the eutectic contents in the die cast AZ91 alloy with the section thicknesses, (a) 2, (b) 6 and (b)10 mm, respectively.

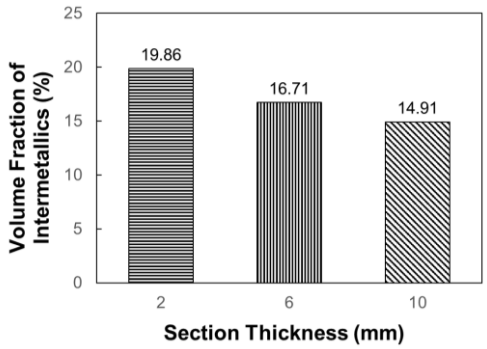

Fig. 10. Volume fraction of eutectics varying with the section thickness.

D. Tensile Properties

The variation of engineering tensile properties including UTS, YS, e_f, tensile toughness and resilience with the section thicknesses are compiled in Table II. The UTS and YS decreases to 129 and 110 MPa for 10 mm thick specimens; from 245 and 169 MPa for the 2 mm coupons, which implies over 50% reduction in UTS and almost 35% decrease in YS, respectively. Moreover, the elongations are 4.07%, 3.04% and 0.73% for the 2, 6, and 10 mm specimens, respectively, indicate evidently that a significant decrease in elongation occurs when the section thickness of specimens increases. The results of the current study is consistent with the relationship between tensile properties and section thicknesses for different types of die casting magnesium alloys reported in the literature [7]-[9]. As mentioned above, differences in the porosity level and the microstructure of die cast AZ91 should be responsible for the deviation in strengths and elongation. The fine dendritic structure, high volume fractions of eutectics and low porosity level of the thin specimens enhances their tensile properties. The relatively low strengths and elongations of the thick specimens result from the coarse dendritic structure, low volume fractions of eutectics, thin skin layer, high porosity level in the center, and the presence of large pores.

TABLE II: TENSILE PROPERTIES OF THE DIE CAST AZ91 ALLOY AT ROOM TEMPERATURE

Section Thickness (mm)	UTS (MPa)	YS (MPa)	e_f (%)	Modulus (GPa)
2	245.54	169.26	4.07	37.8
6	182.91	132.02	3.04	28.6
10	129.17	110.59	0.73	25.9

E. Deformation Behavior

1) Resilience

The ability of a material to absorb energy is referred to as resilience when it is deformed elastically, and releases that energy upon unloading. The resilience is usually measured by the modulus of resilience which is defined as the maximum strain energy absorbed per unit volume without creating a permanent distortion. It can be calculated by integrating the stress-strain curve from zero to the elastic limit. In uniaxial tension, the strain energy per unit volume can be determined by the following equation:

$$U_r = \frac{(YS)^2}{2E} \quad (3)$$

where U_r is the modulus of resilience, *YS* is the yield strength, and *E* is the Young's modulus. The calculated moduli of resilience for different section thickness of AZ91 are given in Table III. In comparison between 2 mm and 10 mm specimens, the modulus of resilience in 2 mm is 140 kJ/m^3 higher than that of the 10 mm. This implies that the AZ91 in the 2mm thickness is much more capable of resisting energy loads in engineering application during service, in which no permanent deformation and distortion are allowed.

2) Toughness

The tensile toughness of a ductile alloy is its ability to absorb energy during static loading condition, i.e., static deformation with a low strain rate. The ability to bear applied stresses higher than the yield strength without fracturing is usually required for various engineering applications. The toughness for ductile alloys can be considered as the total area under the stress-strain curve for the amount of the total energy per unit volume. To evaluate the deformation behavior, the energy expended in deforming a ductile alloy per unit volume given by the area under the stress-strain curve can be approximated by

$$U_t = U_{el} + U_{pl} = \frac{(YS + UTS)}{2} \times e_f \quad (4)$$

where U_t is the total energy per unit volume required to take to point of fracture, U_{pl} is the energy per unit volume for elastic deformation, and U_{el} is the energy per unit volume for plastic deformation, and e_f is the elongation at fracture. Table III lists the calculated values of the U_t for AZ91 with different section thickness. Examination of the U_t values reveals that the 2 mm specimen exhibits an U_t value of 8.34 MJ/m^3 higher than the 6 mm and the 10 mm specimen. This is because the 2 mm AZ91 alloy has a higher ultimate tensile strength and a greater elongation. As a result, the total area under the stress and strain curve is much larger for the 2 mm specimen.

TABLE III: TENSILE TOUGHNESS AND RESILIENCE OF DIE CAST AZ91 AT ROOM TEMPERATURE

Section Thickness (mm)	Toughness (MJ/m^3)	Resilience (kJ/m^3)
2	8.34	378.95
6	4.78	304.71
10	0.89	236.10

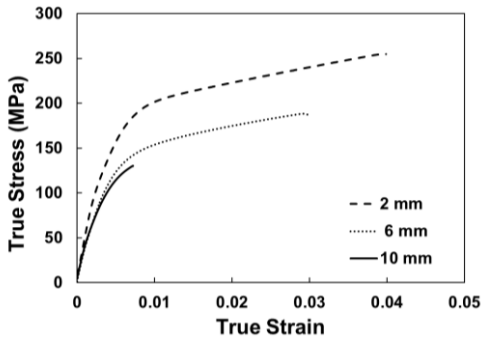

Fig. 11. Typical true strain vs. stress curves for the die cast AZ91 alloy.

Fig. 11 shows the representative true stress and strain curves of the die cast AZ91 alloy. For all three section thicknesses of specimens, the stress variation with the strain follows almost the same pattern. Under tensile loading, the alloy deformed elastically first. Once yield points reach, plastic deformation of the alloy sets in. However, the fracture of the 2 mm-thick specimen occurs at a much higher stress and elongation than that for the 6 and 10 mm thick specimens.

The stress-strain curve for metals is often described by the power expression

$$\sigma = K\varepsilon^n \quad (5)$$

where are *K* and *n* are empirical constants. The regression analysis indicates that the power expression is in a reasonable agreement with the tensile results. The numerical values of these constants in equation (5) with the regression coefficients are listed in Table IV. Equation (5) can be differentiated to obtain strain-hardening rates ($d\sigma/d\varepsilon$).

TABLE IV: BEST FITS PARAMETERS FOR POWER EQUATIONS

Section Thickness (mm)	K (MPa)	n	R^2
2	449.58	0.1176	0.96
6	388.66	0.2039	0.98
10	386.51	.2208	0.99

The strain-hardening behaviors of the die cast AZ91 alloy are illustrated in a plot of strain-hardening rate (dσ/dε) vs true plastic strain (ε) during the plastic deformation as shown in Fig. 12, which is derived from Fig. 11. The 2 mm specimen has a high strain hardening rate (5500 MPa) with respect to that of the thick 10 mm specimen (4600 MPa) at the onset of plastic deformation. It is evident that, despite of decreasing with an increase in true strain, the strain-hardening rates during the plastic deformation of the die cast alloys varies with their section thicknesses. As the section thickness decreases, the strain hardening rates increase. This observation implies that, compared to the 6 and 10 mm thick samples, the die cast AZ91 alloy with the thin cross section (2 mm) is capable of spontaneously strengthening itself increasingly to a large extent, in response to extensive plastic deformation prior to fracture. The low porosity level and the even dispersion of fine intermetallic particles inside grains and around ground boundaries observed by Zhou *et al.* [11], which resist slip in the primary phase should be responsible for the relatively high strain-hardening rate of the thin alloy in the early stage of plastic deformation, i.e., instantly after the onset of plastic flow as indicated in Fig. 11.

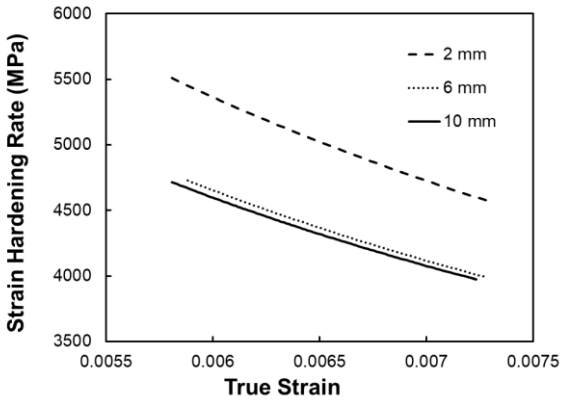

Fig. 12. Strain hardening rate vs. true strain for plastic deformation of the die cast AZ91 alloy.

F. Fracture Characteristics

Examination of the fracture surfaces of tensile specimens via SEM manifests the fracture behavior of die cast AZ91 with three different thicknesses, which is shown in Fig.

13-Fig. 15. The circled areas are observed under a high magnification in an attempt to reveal detailed features of fracture surface and determine the manner where the primary crack originated. The analysis of SEM fractography shows that the fracture behavior of die cast AZ91 is influenced by the section thicknesses. As the section thickness increases, the fracture of AZ91 tends to transit from ductile to brittle mode.

The fracture surface of the 2 mm thick specimen illustrated in Fig. 13 is primarily ductile in nature, which is characterized by the presence of deep dimples. The fractograph with a higher magnification, Fig. 13 (b), portrays the dimples with extensive deformation marking along the walls of individual craters. A considerable amount of energy is consumed in the process of the formation of microvoids and microvoid-sheet, eventually leading to the creation of cracks. Thus, this type of fracture failure results from the coalescence of microvoids under the tensile stress. It seems, however, that the failure of the 10 mm-thick specimen is caused by a combined brittle fracture mechanism of void coalescence and intergranular fracture (Fig. 15). The similar mechanism for the fracture of die cast magnesium alloys has also been reported in references 11 and 12.

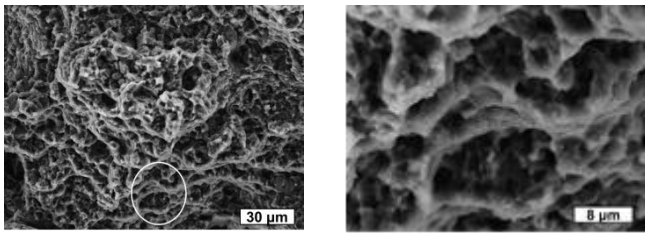

(a) (b)

Fig. 13. SEM fractographs of the 2 mm-thick die cast coupon, (a) low and (b) high magnifications.

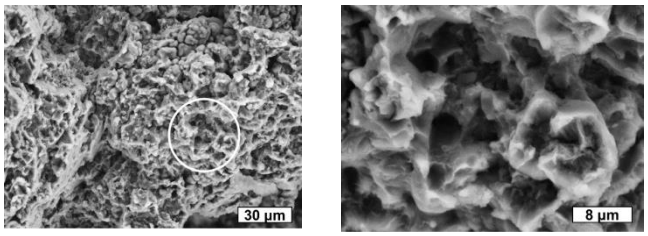

(a) (b)

Fig. 14. SEM fractographs of the 6 mm-thick die cast coupon, (a) low and (b) high magnifications.

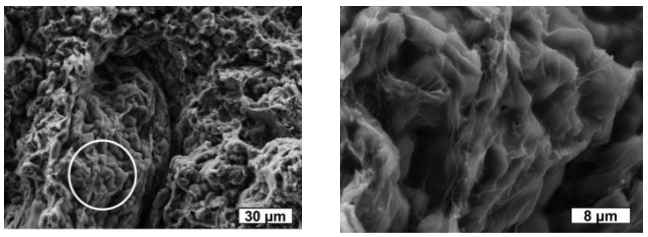

(a) (b)

Fig. 15. SEM fractographs of the 10 mm-thick die cast coupon, (a) low and (b) high magnification.

IV. Conclusion

The strain-hardening and fracture failure of the high pressure die cast magnesium alloy AZ91 is influenced by its section thickness. The results of tensile testing indicate that the mechanical properties, UTS, YS, and e_f, as well as resilience (U_r) and toughness (U_t) increase significantly with a reduction in the section thickness of the alloy. The analysis of plastic deformation behavior reveals that, an increase in high strain-hardening rates of the alloy with decreasing the section thickness enables the alloy to spontaneously strengthen the materials increasingly to a large extent, in response to extensive plastic deformation prior to fracture. The observation via SEM fractography illustrates that the fracture behavior of die cast AZ91 is influenced by the section thickness. As the section thickness increases, the fracture of AZ91 tends to transit from ductile to brittle mode.

Conflict of Interest

The authors declare no conflict of interest.

Author Contributions

The first author was in charge of manuscript organization, experimental preparation and result analyses. The assistance in experimental work was provided by the 2nd and 3rd authors. The corresponding author, Henry Hu, supervised the entire research project and finalized the manuscript. All the authors had approved the final version of the manuscript for publication.

Acknowledgements

The authors would like to take this opportunity to thank the Natural Sciences and Engineering Research Council of Canada for supporting this work.

References

[1] K. Guan, B. Li, Q. Yang, X. Qiu, Z. Tian, D. Zhang, D. Zhang, X. Niu, W. Sun, X. Liu, and J. Meng, "Effects of 1.5wt% samarium(Sm) addition on microstructures and tensile properties of a Mg-6.0Zn-0.5Zr alloy," *J. Alloys and Compounds*, vol. 735, pp. 1737, 2018.

[2] Y. Y. Li, W. M. Zhao, J. Ding, and H. T. Xue, "Ignition-proof performance and mechanism of AZ91D-3Nd-xDy magnesium alloys at high temperatures" *China Foundry*, vol. 15, no. 2, 2018, p. 97, 2018.

[3] B. R. Powell, V. Rezhets, M. P. Balogh, and R. A. Waldo, "Microstructure and creep behavior in AE42 magnesium die-casting alloy," *JOM*, vol. 54, p. 34, August 2002.

[4] A. A. Luo, "Magnesium casting technology for structural application," *Journal of Magnesium and Alloys*, vol. 1, issue 1, p. 2, March 2013.

[5] M. M. Avedesian and H. Baker, *Magnesium and Magnesium Alloys-ASM Specialty Handbook*, ASM Int., Materials Park, OH, USA, 1999.

[6] M. Zhou, N. Li, and H. Hu, "Effect of section thicknesses on tensile behavior and microstructureof high pressure die cast magnesium alloy AM50," *Mater. Sci. Forum*, vols. 475-479, p. 463, 2005.

[7] C. H. Cáceres, W. J. Poole, A. L. Bowles, and C. J. Davidson, "Section thickness, microhardness and yield strength in high -pressure diecast magnesium alloy AZ91," *Materials Science and Engineering A*, vol. 402, issues (1-2), p. 269, August 2005.

[8] S. L. Sin, D. Dubé, and R. Tremblay, "An investigation on microstructural and mechanical properties of solid mould investment casting of AZ91D magnesium alloy," *Materials Characterization*, vol. 59, issues 2, p. 178, February 2008.

[9] H. T. Gjestland, S. Sannes, H. Westengen, and D. Albright, "Effect of casting temperature, section thickness and die filling sequence on microstructure and mechanical properties of high pressure die castings," *Dies Casting Engineering*, vo. l48, no. 4, p. 56, 2004.

[10] M. Zhou, "An experimental study of die and squeeze cast magnesium alloy AM50,"M.S. thesis, Dept. Mechanical, Automotive, and Material, Univ. of Windsor, Windsor, Ontario, Canada, 2004.

[11] Z. Sun, M. Zhou, N, Li, and H. Hu, "Strain-Hardening and Fracture Behavior of Die Cast Magnesium Alloy AM50," *Adv. Mater. Sci. Eng.*, 2007.

[12] M. Zhou, N. Li, J. Lo, and H. Hu, "Microstructure and tensile properties of squeeze cast magnesium alloy AM50," *J. Mater. Eng. Perform.*, vol. 14, no. 4, p. 539, 2005.

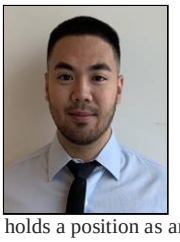

Zixi Sun was born in Moscow, Russia in 1993. He obtained his master and bachelor degrees in the engineering materials program at the University of Windsor, Windsor, Ontario, Canada, in 2017 and 2019.

He has been working in the field of light alloy development for the automotive industry since the 2017. He has published three papers in refereed journal and conference proceedings. He currently holds a position as an engineer at the Hexcel Corporation, Shanghai, China.

Xinyu Geng was born in Daqing, China in 1991. He obtained his master and bachelor degrees in the engineering materials program at the University of Windsor, Windsor, Ontario, Canada, in 2015 and 2019.

He has been working in the field of surface treatment of light alloys for the automotive industry since 2015. He is currently working as a product engineer in Ford Motor Company, Windsor, Ontario, Canada.

Luyang Ren has been a PhD student in engineering materials at the University of Windsor since 2017 and has published over ten papers in refereed journal and conference proceedings. His research interest focused on modeling interfacial heat transfer coefficient between mould and casting alloy for simulating solidification process during indirect squeeze casting of light alloys used in automotive industry. He obtained master of applied science of electrical and computer engineering in University of Waterloo in 2002 and bachelor of engineering of materials science and engineering from University of Science and Technology Beijing in 1985.

Henry Hu was born on March 20, 1964 in Shanghai, China. He received Ph.D. degree from University of Toronto in 1996, M.A.Sc. degree from University of Windsor in 1991, and B.A.Sc. degree from Shanghai University of Technology in 1985. His current research is on materials processing and evaluation of light alloys and composites. His recent fundamental research is focussed on transport phenomena and mechanisms of solidification, phase transformation and dissolution kinetics. His applied research has included development of magnesium automotive applications, cost-effective casting processes for novel composites, and control systems for casting processes.

He was a NSERC industrial research fellow from 1995 to 1997. His publications are in the area of magnesium alloys, composites, metal casting, computer modelling, and physical metallurgy. He was a key reader of the Board of Review of Metallurgical and Materials Transactions, a committee member of the Grant Evaluation Group for Natural Sciences and Engineering Research Council of Canada, National Science Foundation (USA) and Canadian Metallurgical Quarterly. He has served as a member or chairman of various committees for CIM-METSOC, AFS, and USCAR. He is a tenured full professor at Department of Mechanical, Automotive & Materials Engineering, University of Windsor. He was a senior research engineer at Ryobi Die Casting (USA), and a chief Metallurgist at Meridian Technologies, and a research scientist at Institute of Magnesium Technology.